Monthly Notices of the Royal Astronomical Society

# The Schmidt-Kennicutt law, the star formation efficiency, and the mass density of clusters from gravitational collapse rather than turbulent support

| | |
|---|---|
| Journal: | *Monthly Notices of the Royal Astronomical Society* |
| Manuscript ID | MN-24-1353-MJ |
| Manuscript type: | Main Journal |
| Date Submitted by the Author: | 20-Jun-2024 |
| Complete List of Authors: | Zamora, Manuel; Instituto Nacional de Astrofisica Optica y Electronica, ; Universidad Nacional Autonoma de Mexico Centro de Radioastronomia y Astrofisica,<br>Camacho, Vianey; Universidad Nacional Autonoma de Mexico Instituto de Radioastronomia y Astrofisica,<br>Ballesteros-Paredes, Javier; UNAM, Instituto de Radioastromia y Astrofisica;<br>Vázquez-Semadeni, Enrique; Universidad Nacional Autonoma de Mexico, Instituto de Radioastronomia y Astrofisica<br>Palau, Aina; Universidad Nacional Autonoma de Mexico, Instituto de Radioastronomía y Astrofísica<br>Román-Zúñiga, Carlos; Universidad Nacional Autonoma de Mexico Instituto de Astronomia Campus Ensenada, Instituto de Astronomía<br>Hernández-Cruz, Andrés; Instituto Nacional de Astrofisica Optica y Electronica<br>Gómez, Gilberto; Universidad Nacional Autónoma de México, Instituto de Radioastronomia y Astrofisica<br>Quesada-Zúñiga, Fabián; Instituto Nacional de Astrofisica Optica y Electronica |
| Keywords: | galaxies: star formation < Galaxies, ISM: clouds < Interstellar Medium (ISM), Nebulae, Galaxy: fundamental parameters < The Galaxy |
| | |

MNRAS 000, 1–13 (2023) Preprint 20 June 2024 Compiled using MNRAS LATEX style file v3.0

# Gravity or turbulence? VII. The Schmidt-Kennicutt law, the star formation efficiency, and the mass density of clusters from gravitational collapse rather than turbulent support

Manuel Zamora-Avilés[1]★, Vianey Camacho[2], Javier Ballesteros-Paredes[2], Enrique Vázquez-Semadeni[2], Aina Palau[2], Carlos Román-Zúñiga[3], Andrés Hernández-Cruz[1], Gilberto C. Gómez[2], Fabián Quesada-Zúñiga[1], and Raúl Naranjo-Romero[1]

[1]*Instituto Nacional de Astrofísica, Óptica y Electrónica, Luis E. Erro 1, 72840 Tonantzintla, Puebla, México*
[2]*Instituto de Radioastronomía y Astrofísica, UNAM, Apartado Postal 3-72, 58089 Morelia Michoacán, México*
[3]*Instituto de Astronomía, Universidad Nacional Autónoma de México, Unidad Académica en Ensenada, Ensenada 22860 BC, México*

Last updated 2020 June 10; in original form 2013 September 5

## ABSTRACT

We explore the Schmidt-Kennicutt (SK) relations and the star formation efficiency per free-fall time ($\epsilon_{\rm ff}$), mirroring observational studies, in numerical simulations of filamentary molecular clouds undergoing gravitational contraction. We find that *a)* collapsing clouds accurately replicate the observed SK relations for galactic clouds and *b)* the so-called efficiency per free-fall time ($\epsilon_{\rm ff}$) is small and constant in space and in time, with values similar to those found in local clouds. This constancy is a consequence of the similar radial scaling of the free-fall time and the internal mass in density structures with spherically-averaged density profiles near $r^{-2}$. We additionally show that *c)* the star formation rate (SFR) increases rapidly in time; *d)* the low values of $\epsilon_{\rm ff}$ are due to the different time periods over which $\tau_{\rm ff}$ and $\tau_{\rm YSO}$ are evaluated, together with the fast increasing SFR, and *e)* the fact that star clusters are significantly denser than the gas clumps from which they form is a natural consequence of the fast increasing SFR, the continuous replenishment of the star-forming gas by the accretion flow, and the near $r^{-2}$ density profile generated by the collapse Finally, we argue that the interpretation of $\epsilon_{\rm ff}$ as an efficiency is problematic because its maximum value is not bounded by unity, and because the total gas mass in the clouds is not fixed, but rather depends on the environment where clouds are embedded. In summary, our results show that the SK relation, the typical observed values of $\epsilon_{\rm ff}$, and the mass density of clusters arise as a natural consequence of gravitational contraction.

**Key words:**

## 1 INTRODUCTION

The Schmidt-Kennicutt (SK) relation is a fundamental correlation in astrophysics that has important implications for our understanding of how galaxies form stars and evolve. In its classical form is an empirical relation between the surface densities of the star formation rate ($\Sigma_{\rm SFR}$) and the gas mass ($\Sigma_{\rm gas}$). It was first proposed by Schmidt (1959) and confirmed observationally by Kennicutt (1998). The relation has a power law form $\Sigma_{\rm SFR} \propto \Sigma_{\rm gas}^N$, where the exponent $N$ is typically between 1 and 2 for extragalactic studies (see the review by Kennicutt & Evans 2012; Sun et al. 2023, and references therein), but around 2 or larger for individual molecular clouds (Gutermuth et al. 2011; Pokhrel et al. 2021).

Here, we focus on individual molecular cloud (MC) observational determinations of the SK relation with the more reliable determination of the star formation rate (SFR) based on direct young stellar objects (YSO) counts (see, e.g., Gutermuth et al. 2011; Lada et al. 2013; Evans et al. 2014; Lombardi et al. 2014; Heyer et al. 2016; Zari et al. 2016; Ochsendorf et al. 2017; Lada et al. 2017; Pokhrel et al. 2021).[1] These observations produce a classical $\Sigma_{\rm SFR} \propto \Sigma_{\rm gas}^N$ SK relation with an exponent $N \sim 2$ with some dispersion.

From the very definition of star formation rate, one can derive a fundamental form of the star formation law (see, e.g., Ballesteros-Paredes et al. 2023, for a formal derivation),

$$\mathrm{SFR} = \epsilon_{\rm ff}\left(\frac{M_{\rm gas}}{\tau_{\rm ff}}\right), \tag{1}$$

where $M_{\rm gas}$ is the mass in gas, $\epsilon_{\rm ff}$ a parameter known as the *star formation efficiency per free-fall time*,[2] and $\tau_{\rm ff}$ is the free-fall time

[1] Other works based on indirect determinations of the SFR give SK relation with a wide dispersion (e.g., Lee et al. 2016; Gallagher et al. 2018).
[2] Traditionally, $\epsilon_{\rm ff}$ has been called the star formation efficiency per free-fall time. However, we prefer to call it the *ratio of the SFR to the gas-infall rate, since,* as we will discuss in §4.1.2, its interpretation as an efficiency is problematic. Nonetheless, we keep its traditional symbol, $\epsilon_{\rm ff}$, for clarity.

★ Contact e-mail: mzamora@inaoep.mx

given by

$$\tau_{\rm ff} = \sqrt{\frac{3\pi}{32G\rho}}, \tag{2}$$

with $\rho$ the mean mass density of the system. On the other hand, we can write $\epsilon_{\rm ff}$ as

$$\epsilon_{\rm ff} = \frac{\rm SFR}{M_{\rm gas}/\tau_{\rm ff}} = \frac{\tau_{\rm ff}}{\tau_{\rm depl}}, \tag{3}$$

with $\tau_{\rm depl}$ being the depletion time, which is the time to exhaust the current gas mass, given the current star formation rate $dM_*/dt$,

$$\tau_{\rm depl} = \frac{M_{\rm gas}}{\rm SFR}. \tag{4}$$

Eq. (1) has been proposed based on theoretical and empirical arguments elsewhere (e.g., Krumholz & Tan 2007; Krumholz et al. 2012; Lee et al. 2016; Vutisalchavakul et al. 2016; Elmegreen 2018; Pokhrel et al. 2021; Sun et al. 2023).

Observationally, the star formation rate of a molecular cloud in the Solar Neighbourhood is approached as the amount of mass present in some type of protostar, divided by the characteristic lifetime of those protostars, $\tau_{\rm YSO}$,

$$\langle {\rm SFR} \rangle_{\tau_{\rm YSO}} = \frac{M_*}{\tau_{\rm YSO}}. \tag{5}$$

Observations in the last decade towards Milky Way molecular clouds have reported values of $\epsilon_{\rm ff}$ in the range of 0.006-0.06 (e.g., Lada et al. 2013; Evans et al. 2014; Heyer et al. 2016; Ochsendorf et al. 2017). More recently, using complete counts of protostellar objects to estimate SFR and Herschel observations to estimate the surface density of molecular clouds in the Solar Neighbourhood, each at different levels of its hierarchy, Pokhrel et al. (2021) showed that the surface density of star formation rate correlates, on the one hand, linearly with the ratio of the surface density of molecular gas ($\Sigma_{\rm mol}$) divided by its free-fall time,

$$\Sigma_{\rm SFR} \propto \frac{\Sigma_{\rm mol}}{\tau_{\rm ff}}, \tag{6}$$

but on the other, quadratically with the surface density of the gas alone,

$$\Sigma_{\rm SFR} \propto \Sigma_{\rm mol}^2. \tag{7}$$

In addition, they also showed that the ratio of the SFR to the gas-infall rate, measured for different surface density thresholds within a single cloud, is nearly independent of the surface density, and that the set of clouds exhibits values of $\epsilon_{\rm ff}$ in the range

$$\epsilon_{\rm ff} \in (0.1, 0.01), \tag{8}$$

with a mean value of $\epsilon_{\rm ff} \sim 0.03$. It is worth noting that the modified version of the SK lawin terms of the $\Sigma_{\rm mol}/\tau_{\rm ff}$ (eq. 6 Genzel et al. 2010; Krumholz et al. 2012), can be viewed in general as a two-parameter relation of the form

$$\log \Sigma_{\rm SFR} = \log \epsilon_{\rm ff} + N_2 \log \left( \frac{\Sigma_{\rm mol}}{\tau_{\rm ff}} \right), \tag{9}$$

with $N_2$ the exponent ($N_2 = 1$ in eq. 6) and $\epsilon_{\rm ff}$ the intercept.

The long depletion times implied by the ratio $\Sigma_{\rm gas}/\Sigma_{\rm SFR}$ ($\sim 10^9$ yr for galaxies, and $\gtrsim 10^7$ for local molecular clouds, see Kennicutt 1998; Bigiel et al. 2008; Pokhrel et al. 2021) have been used to argue that star formation is a slow process (e.g., Krumholz & Tan 2007; Evans et al. 2021, 2022), with clouds being dominated by turbulence (Ostriker et al. 2010; Evans et al. 2022). In this scenario, so-called gravo-turbulent (GT), MCS are in a quasi-equilibrium state between turbulence and self-gravity and, therefore, have long lifetimes ($\gg \tau_{\rm ff}$) and a stationary low SFR (e.g., Mac Low & Klessen 2004; Krumholz & McKee 2005; Ballesteros-Paredes et al. 2007; McKee & Ostriker 2007; Krumholz & McKee 2020). On the other hand, there is the global hierarchical collapse (GHC) model (Vázquez-Semadeni et al. 2009, 2019), in which the gas in MCs is continuously flowing from the low-density towards the star-forming sites. In this model, the clouds evolve by growing in mass and size (Heitsch & Hartmann 2008; González-Samaniego & Vazquez-Semadeni 2020; Camacho et al. 2020) by accretion from their surrounding material, increase their SFR (Hartmann et al. 2012; Zamora-Avilés et al. 2012; Zamora-Avilés & Vázquez-Semadeni 2014) and their massive-star content (Hartmann et al. 2012; Vázquez-Semadeni et al. 2017, 2023), and their lifetimes are determined by the time required to form stars sufficiently massive to interrupt the local SF episode and disperse the local gas.

In the former scenario, it has been shown that, indeed, the parameter $\epsilon_{\rm ff}$ can be small ($\simeq 0.01$). But, more importantly, $\epsilon_{\rm ff}$ depends on the virial parameter (e.g., Padoan et al. 2012; Kim et al. 2021). Since a single cloud exhibits a variety of virial parameter values at different levels of its hierarchy (at low surface densities, the virial parameter is typically large and approaches 1–2 at large surface densities, see Figs. 1 and 2 in Evans et al. 2021), it is hard to reconcile the constancy of $\epsilon_{\rm ff}$ found by Pokhrel et al. (2021) in the GT model.

The SK law and the parameter dependence of $\epsilon_{\rm ff}$ in the context of collapsing clouds with stellar feedback have been investigated recently. For example, both Kim et al. (2021) and Suin et al. (2023) studied the behaviour of $\epsilon_{\rm ff}$ for isolated, collapsing spherical clouds under the influence of feedback mechanisms. The former authors found that the $\epsilon_{\rm ff}$ depends inversely on the initial virial parameter, and both works found that the value of $\epsilon_{\rm ff}$ is strongly affected by the feedback and magnetic fields. Although we agree that stellar feedback is crucial in interrupting the star formation process, in the previous paper of this series, Ballesteros-Paredes et al. (2023) have shown that the three results found by Pokhrel et al. (2021) (Eqs. [6]-[8]), as well as the correlations shown in extragalactic studies (e.g., Kennicutt 1998; Gao & Solomon 2004; Wu et al. 2005; Bigiel et al. 2008; Sun et al. 2023) can be understood simply as a consequence of the collapse of molecular clouds. In order to support this view, in the present contribution, we study the SK relation and the ratio of the SFR to the gas-infall rate in numerical simulations of collapsing molecular clouds, following a methodology similar to that used for observations of local clouds. In §2 we describe the numerical simulations used in our analysis, which correspond to two filamentary structures. In §3 we present the results related to the SK relations and the parameter $\epsilon_{\rm ff}$. In §4 we discuss the implications of our results, while §5 presents our main conclusions.

## 2 NUMERICAL METHODS

In this work, we study the SK relations in dense (molecular) structures dominated by self-gravity in the GHC scenario using three-dimensional magnetohydrodynamical (MHD) numerical simulations.

We used two different models of filamentary clouds undergoing collapse, which we refer to as the Filament simulation (FS) and the

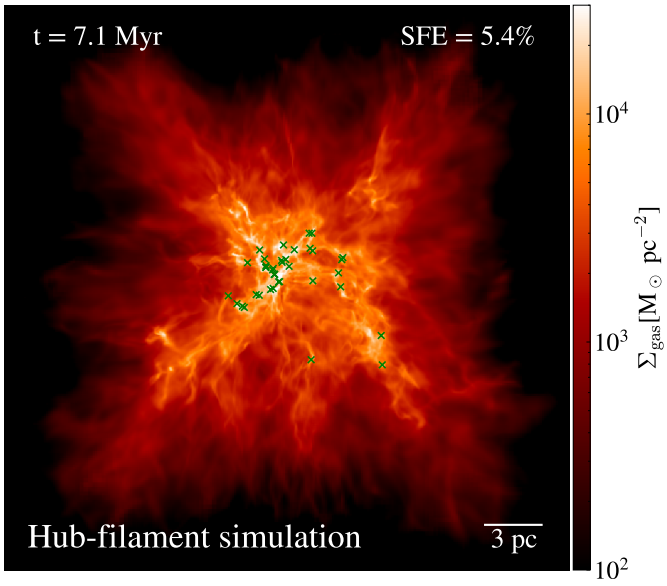


**Figure 1.** Gas surface density of the "Hub-filament" simulation at $t$ =7.1 Myr, time at wich the **star formation efficiency** is 5.4% **(see the text)**. The green crosses (sink particles) represent groups of stars.

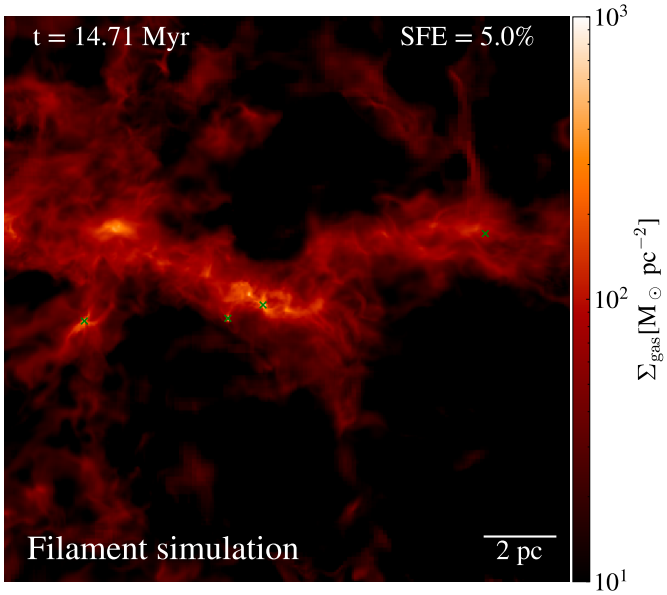


**Figure 2.** Gas surface density of the "Filament" simulation at $t$ = 14.7 Myr, time at wich the star formation efficiency is 5%. The green crosses (sink particles) represent groups of stars.

Hub-Filament simulation (HFS). Both models include MHD, self-gravity, and formation of sink particles. These sets of simulations were performed with the AMR FLASH code (Fryxell et al. 2000). We use the MHD HLL3R solver (Waagan et al. 2011) to solve the ideal MHD equations, ensuring a balance between accuracy and robustness, useful characteristics for highly supersonic astrophysical problems. To solve the Poisson equation for the self-gravity of the gas, we use an OctTree solver (Wünsch et al. 2018). We refine dynamically following the Jeans criterion (Truelove et al. 1997). A sink particle can be formed once a given cell reaches the maximum allowable refinement level and its density exceeds a specific density threshold ($\rho_{\rm thr}$). The formation of the sink particle involves multiple checks within a spherical control volume (of radius 2.5 times the size of the cell at the maximum level of refinement, $\Delta x$) around the cell of interest: 1) the gas is converging (negative divergence), 2) there is a minimum in the gravitational potential, 3) the cell is Jeans unstable, 4) it is gravitationally bound (negative total energy), and 5) the cell is not within the accretion radius of another sink (Federrath et al. 2010). The sink is created using the excess mass within the cell (that is, $M_{\rm sink} = (\rho - \rho_{\rm thr})\Delta x^3$) and is capable of accreting mass from its surrounding environment. Note that given the size of the regions and the resolution of our simulations, a sink particle in both models represents a group of stars rather than an individual star. Further details of the two simulations are as follows:

**Hub-Filament simulation (HFS)**. This simulation was first presented in Juárez et al. (2017),[3] and follows the collapse of a cloud with an initial turbulent velocity field and constant density. Since the simulation is isothermal, we re-scale it to match the properties of local molecular clouds in the Solar Neighborhood. Thus, our simulation can be pictured as a hub-filament system with an initial linear size of 29.4 pc and an initial density of $n \sim 20$ cm$^{-3}$. This implies that, given a temperature of 10 K, the total mass is about ~234 Jeans masses, with a total gass mass of $2.94 \times 10^4\ M_\odot$. After ~0.94 $\tau_{\rm ff}$, the linear size of its filaments converging to the central hub is about ~ 10 pc (see Fig. 1), comparable to the Monoceros molecular cloud (see, e.g., Treviño-Morales et al. 2019).

Because the simulation contains over two hundred Jeans masses, it is prone to gravitational fragmentation. The initial turbulence in this simulation SEEDS (i.e., determines the location) of the sites of the local collapses, which occur at the same time as the collapse of the whole cloud. Since the initial geometry is a cube, it naturally forms filaments along the diagonals of the cube, with a density gradient towards the center, where a hub system is formed.

**Filament simulation (FS)**. This run was presented in Zamora-Avilés et al. (2018, model labelled as B3J) to study the formation and evolution of magnetised dense structures. The simulation box, with sizes $L_x = 256$, and $L_{y,z} = 128$ pc, is filled with warm neutral gas at a density of 2 cm$^{-3}$ and a temperature of 1450 K. The initial magnetic field is uniform along the $x-$direction with a strength of 3 $\mu$G, so the formed cloud is magnetically supercritical. The thermodynamic behaviour of the ISM is modelled by incorporating heating and cooling processes, using analytic fits from Vázquez-Semadeni et al. (2007), based on cooling functions from Koyama & Inutsuka (2002). This results in a thermally unstable regime for densities 1–10 cm$^{-3}$ and temperatures 500–5000 K.

In this simulation, two cylindrical converging flows of radius $R$ = 32 pc and length $L$ = 112 pc are set to collide at a relative moderately supersonic velocity of 7.5 km s$^{-1}$. This collision forms denser, cold, neutral small clouds at the centre of the box, mainly due to the non-linear thermal instability triggered by the compression. The newborn cloud continues to accrete gas from the cylinders and eventually becomes dense enough to be considered molecular. The resulting morphology of the newborn molecular cloud is characterised by a network of filaments, and in this work, we focus on one particular filament previously analysed by Camacho et al. (2023, see Fig. 2).

[3] See also Zamora-Avilés et al. (2017).

This filament is contained in a sub-box of 16 pc in size and has a time-varying, increasing dense gas mass, going from $\sim 3000 M_\odot$ to $\sim 4000 M_\odot$ at the times when the measurements described below are performed.

In our analysis of both simulations, we define the zero time point as the moment the first sink particle forms, occurring 5.6 Myr and 11.2 Myr after the simulation start for the HFS and FS, respectively. At this zero times, we calculate the free-fall times of 2.97 and 2.87 Myr using the mean density of gas that would be considered molecular (i.e., gas with density $n > 100$ cm$^{-3}$). This corresponds to mean densities of $\langle n(t = 5.6\,\mathrm{Myr})\rangle = 139.8$ and $\langle n(t = 11.2\,\mathrm{Myr})\rangle = 240.9\,\mathrm{cm}^{-3}$, for the HFS and FS, respectively.

In both simulations, as expected from theory (e.g., Franco & Cox 1986; Hartmann et al. 2001), while the compressed gas becomes denser and more massive, the clouds become gravitationally unstable and proceed to collapse. And just as it occurs with a system of particles (e.g., Noriega-Mendoza & Aguilar 2018), the natural outcome of the gravitational collapse of a molecular cloud is to exhibit equipartition between its gravitational and internal energies (see also Vázquez-Semadeni et al. 2007; Noriega-Mendoza & Aguilar 2018; Camacho et al. 2023; Ibáñez-Mejía et al. 2022), which may very well be mistaken as virial equilibrium (Ballesteros-Paredes et al. 2011, 2018; Camacho et al. 2023).

### 2.1 Structure selection and computed quantities

Since we want to mimic the observational procedure to estimate dense gas mass surface densities, we projected the volumetric density along one of the axes. This gives us the mass surface density on the plane defined by in the other two axes. By thresholding this mass surface density, we delineate isocontours of the same surface gas density, inside of which we measure the mass in dense gas, $M_{\rm mol}$, the mass in newborn stars, $M_{\rm sinks}$, and the area $A$. From these quantities, we can compute the size of the cloud ($R$) and the mass density ($\rho$) as

$$R = \sqrt{\frac{A}{\pi}}, \tag{10}$$

$$\rho = \frac{3\pi^{1/2}}{4}\,\frac{M_{\rm mol}}{A^{3/2}}. \tag{11}$$

With this procedure, we can compute different quantities related to SK-type relations:

(i) **The present star formation efficiency (SFE)**. At all times, we estimate the total instantaneous SFE in the raw 3D simulations as

$$\mathrm{SFE} = \frac{M_{\rm sinks}}{M_{\rm mol} + M_{\rm sinks}}, \tag{12}$$

with $M_{\rm sinks}$ being the total mass in sink particles within the projected structure and $M_{\rm mol}$ the dense mass ($n > 100\,\mathrm{cm}^{-3}$).

Furthermore, as pointed out earlier, our simulations do not include stellar feedback. However, to avoid unrealistic results due to its absence, we analyse the simulations at early stages, when the SFE is 2% 5% and 10% (i.e., at $t$ =1.2, 1.5, and 1.7 Myr) for the HFS. For the FS, we analyse times when the SFE is 5% and 10% (i.e., 3.5 and 4.3 Myr).[4]

(ii) **The star formation rate**. We note that in observational works, the SFR is typically estimated as the mass that has gone into some type of proto-stellar object, $M_*$, divided by the typical life span of this type of objects, $\tau_{\rm YSO}$ (e.g., Lada et al. 2010; Pokhrel et al. 2021); that is

$$\mathrm{SFR} \approx \frac{M_*(t)}{\tau_{\rm YSO}}. \tag{13}$$

Observationally, the mass in newborn stars is usually computed as the number of protostellar objects multiplied by the typical mass of the protostar, $\langle M\rangle \sim 0.5\ M_\odot$. In the simulations, we have the advantage of knowing exactly the amount of mass that has gone into sink particles, $M_{\rm sinks}$, so we use this quantity directly, i.e., $M_* = M_{\rm sinks}$ at every timestep.

As for the timescale, characteristic timescales have been estimated for protostellar objects at different stages (e.g., Ward-Thompson et al. 2007; Heiderman & Evans 2015). If the objects to count are generic YSOs, the assumed characteristic timescale is $\tau_{\rm YSO} \sim 2$ Myr (e.g., Evans et al. 2009; Heiderman et al. 2010; Lada et al. 2010). In contrast, when considering embedded protostellar objects, the characteristic timescale is of the order of $\tau_{\rm YSO} \sim 0.5$ Myr (e.g., Pokhrel et al. 2021; Lada et al. 2013). Dib et al. (2024) suggests that using less-evolved embedded objects (Class 0) gives a more reliable estimation of the SFR, especially for a time-dependent burst-like star formation history.

In order to mimic observations, in our simulations we want to compute the mass accreted by sink particles since they first appear. Consequently, we compute $\tau_{\rm YSO}$ as the time spent between the formation of the first sink particle and the time under analysis. In the HFS, $\tau_{\rm YSO}$ is 1.2, 1.5, and 1.7 Myr for SFEs of 2%, 5%, and 10%, respectively. In the FS, $\tau_{\rm YSO}$ reaches 3.4 and 4.2 Myr at SFEs of 5% and 10%, respectively.

(iii) **The ratio of the SFR to the gas-infall rate** ($\epsilon_{\rm ff}$). This parameter can be computed as the ratio between the averaged SFR (Eq. 13) and the free-fall collapse rate, ($M_{\rm mol}/t_{\rm ff}$), with $M_{\rm mol} = \Sigma_{\rm mol} * A$ (e.g., Ballesteros-Paredes 2023).

## 3 RESULTS

Our ultimate goal is to understand the origin of the Schmidt-Kennicutt relation, the constancy of $\epsilon_{\rm ff}$, and its observed low value ($\epsilon_{\rm ff} \sim 3 \times 10^{-2}$). For this purpose, in this section we analyze, for each one of our simulations, the evolution of the present star formation efficiency, the SK relations, and the ratio of the star formation rate to the gas-infall rate, $\epsilon_{\rm ff}$[5].

### 3.1 The Star Formation Rates and the Present Star Formation Efficiency

Fig. 3 shows the time history of the SFE (eq. 12) for the HFS (left panel) and the FS (right panel) runs, measured from the 3D row simulations. These measurements are derived from the three-dimensional raw simulation data. The upper axes of this figure show the time in units of the corresponding free-fall times (see §2).

[4] For the FS, we do not analyse the time at which the SFE is 2% since it only has two sinks.

[5] We avoid to use the term "efficiency per free-fall time" because as we explain in §1, it is clear it is not an efficiency.

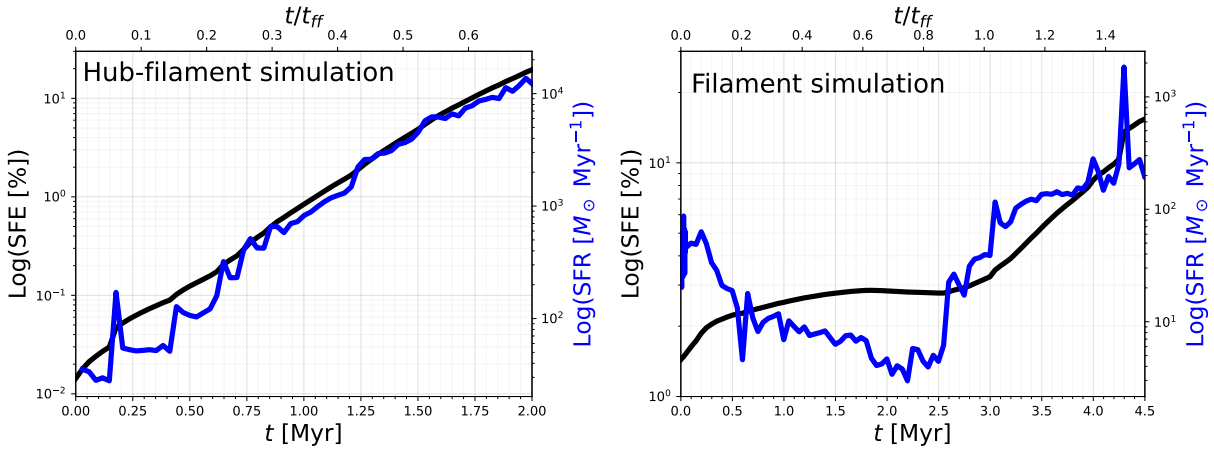


**Figure 3.** Star formation efficiencies (black lines) and star formation rates (blue lines) as a function of time for the Hub-filament system (left) and the Filament (right). The top axes show the time in units of the free-fall time. We set the zero time at the onset of sink formation and calculate the free-fall time using the mean density of dense gas (with $n > 100\,\mathrm{cm}^{-3}$) at this time (see §3.1).

As can be seen, in both cases, the present SFE increases over time, reaching large values within one free-fall time of the initial gas density. This is due to the lack of stellar feedback in both simulations. Although both curves look similar, they exhibit an important difference. The HFS (panel a) simulation reaches 20% efficiency within a fraction of the free-fall time. In contrast, the FS (panel b) takes twice that time (in units of the free-fall time) to reach a similar value.

Fig. 3 also shows the SFR over time (blue solid lines, right $y$ axes). Similarly to the SFE, the SFR exhibits substantial growth in both cases, although in the FS case (see Sect. 4.1.3), the growth is modulated by accretion flows into the cloud from larger scales, which provide a strong increase in gas mass at the lower levels of the densities of the clouds, without an instantaneous increase of star formation, which takes longer to occur. The substantial growth of the SFE is the product of gravitational collapse, and it is sustained until feedback from massive stars destroys and disperses the cloud (Zamora-Avilés et al. 2012; Colín et al. 2013; Kim et al. 2021; Suin et al. 2023).

It is important to note that the masses of real molecular clouds hardly remain constant as they evolve. As numerical work has shown since long ago, molecular clouds are in a continuous dynamical exchange of mass, momentum, and energy with their surroundings (e.g., Bania & Lyon 1980; Vazquez-Semadeni et al. 1995; Ballesteros-Paredes et al. 1999a). In particular, molecular clouds are likely to be formed by the convergence of large-scale diffuse flows (Ballesteros-Paredes et al. 1999a; Hennebelle & Pérault 1999; Heitsch et al. 2005; Vázquez-Semadeni et al. 2006), and as a natural consequence, their masses evolve continuously (e.g., Heitsch & Hartmann 2008; Vázquez-Semadeni et al. 2009; Zamora-Avilés et al. 2012; Zamora-Avilés & Vázquez-Semadeni 2014). In the FS, the mass of gas with number density grater that $100\,\mathrm{cm}^{-3}$ is $\sim 2.4 \times 10^3\,M_\odot$ at the onset of star formation and increases to $\sim 3 \times 10^3\,M_\odot$ when the SFE reaches 10%. Indeed, in both of our simulations, the dense (with $n > 100\,\mathrm{cm}^{-3}$) gas mass increases over time, as it accretes from its lower-density surroundings. This has the important consequence that, although the stellar mass increases over time, so does the dense gas mass, and therefore the instantaneous SFE does not increase as much (see also González-Samaniego & Vazquez-Semadeni 2020).

### 3.2 SK type relations of collapsing clouds

Our main goal in this contribution is to locate our clouds in the $\Sigma_{\rm SFR} - \Sigma_{\rm mol}$ and $\Sigma_{\rm SFR} - \Sigma_{\rm mol}/\tau_{\rm ff}$ diagrams. Thus, we need to compute the area, SFR, gas mass, and free-fall time at each closed contour as we described in §2.1. As explained before, we compute $\tau_{\rm YSO}$ as the time since the formation of the first sink to the time when the analysis is performed, corresponding to total efficiencies of 2%, 5%, and 10%. The results are shown in Figs. 4 for the HFS and 5 for the FS. In these figures, we additionally show lines that denote constant depletion time (thin dashed lines with slope equal to one, left panels) and lines denoting constant ratio of SFR to gas-infall rate, $\epsilon_{\rm ff}$ (thin dashed lines with slope equal one, right panels). From these figures, we find the following scalings:[6]

(i) $\Sigma_{\rm SFR} = a\Sigma_{\rm mol}^{N_1}$, where $a$ and $N_1$ are the mean intercept and slope, respectively. $a = 5.2 \times 10^{-5}$ and $N_1 = 1.97$ for the HFS. Similarly, $a = 3.1 \times 10^{-4}$ and $N_1 = 2.03$ for the FS.

(ii) $\Sigma_{\rm SFR} = \langle\epsilon_{\rm ff}\rangle\,(\Sigma_{\rm mol}/\tau_{\rm ff})^{N_2}$, with $\langle\epsilon_{\rm ff}\rangle$ and $N_2$ the mean intercept and slope, respectively. $\langle\epsilon_{\rm ff}\rangle = 0.030$ and $N_2 = 0.94$ for the HFS. Similarly, $\langle\epsilon_{\rm ff}\rangle = 0.045$ and $N_2 = 1.01$ for the FS.

These values are consistent with the slopes reported for resolved clouds (e.g., Pokhrel et al. 2021). In both figures (4 and 5), the grey and light grey bands represent one and two standard deviations, respectively. This indicates that the $\Sigma_{\rm SFR} - \Sigma_{\rm mol}/\tau_{\rm ff}$ relation is tighter than the $\Sigma_{\rm SFR} - \Sigma_{\rm mol}$ relation, as it occurs in observations (Pokhrel et al. 2021).

A third point to notice from the left panels of Figs. 4 and 5 is that, the denser the cloud, the lower the depletion times (left panels), although $\epsilon_{\rm ff}$ remains constant (right panels). We discuss this point further in §4.1.

[6] We use a linear least squares fit in the log-log space.

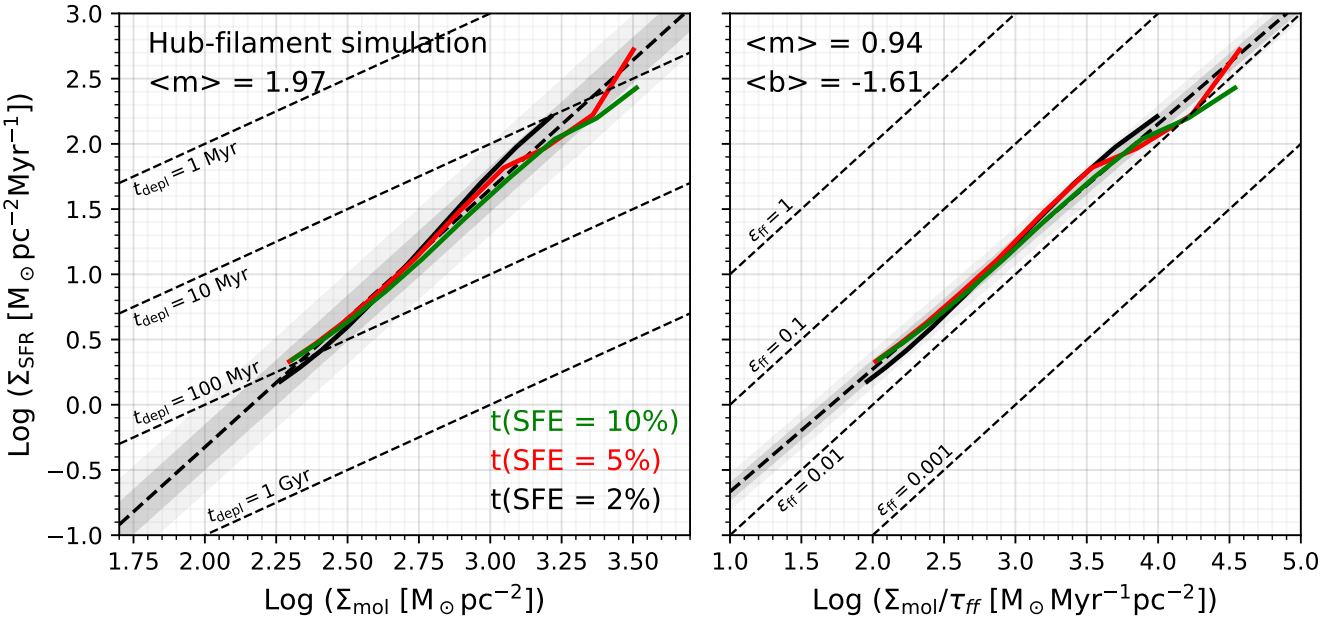


**Figure 4.** The SK relation for the simulated Hub-filament system, quantified at three different times, when the SFE reaches 2%, 5%, and 10% (black, red, and green lines). The left panel shows the relationship $\Sigma_{SFR} - \Sigma_{mol}$, while the right panel shows the relationship and $\Sigma_{SFR} - \Sigma_{mol}/\tau_{ff}$. Each point corresponds to a different surface density isocontour of the same structure. For each set of points we compute the corresponding slope and we show the average ($\langle m \rangle$) of all of them on the top left corner of each panel (as wel as the corresponding intercept ($\langle b \rangle$ in the right panel). The grey and light grey bands correspond to one and two times the standar deviation, respectively. The thin dashed lines in the left panel represent, from top to bottom, depletion times $\tau_{depl}$ of 1, 10, 100, and 1000 Myr. Similarly, in the right panel, thin dashed lines represent $\epsilon_{ff}$ of 1, 0.1, 0.01, and 0.001 (from top to bottom).

### 3.3 The ratio of the SFR to the gas-infall rate, $\epsilon_{ff}$

In addition to the SK-type relations, we also compute $\epsilon_{ff}$ (Eq. 3) as described in §2.1, for different surface density thresholds within each cloud. The results are shown in Figs. 6 and 7, for the HFS and the FS, respectively.

Several points are noteworthy in these figures. First, we note that the HFS simulation (Fig. 6) has a significantly smaller value of $\epsilon_{ff}$ ($\sim$ 2%) than the FS ($\epsilon_{ff} \sim$ 5%, Fig. 7), in spite of having a significantly larger instantaneous SFE at a given fraction of the free-fall time ($\sim$ 10% versus $\sim$ 3% at $t \approx 0.6\tau_{ff}$). This suggests that $\epsilon_{ff}$ is not an accurate measure of the actual SFE. Second, we note that $\epsilon_{ff}$ is nearly independent of the surface density threshold, as could be inferred from Figs. 6 and 7. This behaviour is consistent with the fundamental law of star formation (eq. 1). In addition, the range of values computed for the $\epsilon_{ff} \in (0.014, 0.063)$ in both simulations is consistent with the observational counterpart (Pokhrel et al. 2021, green shaded region in Figs. 6 and 7). In addition, we also note that $\epsilon_{ff}$ remains relatively constant over time in both simulations, even though the instantaneous efficiency is increasing from 2% to 5% and 10%. Our results are consistent with those of Pokhrel et al. (2021), who found no systematic difference in $\epsilon_{ff}$ between clouds with different star formation activity. In Sections 4.1.3 and 4.1.4, we explain this behaviour as a direct consequence of gravitational collapse.

## 4 DISCUSSION

### 4.1 Implications of an increasing SFR and a collapse-determined density profile on the measurement and meaning of $\epsilon_{ff}$

#### *4.1.1 The effect of accretion on the estimated structure lifetimes*

For over nearly 50 years, star formation has been known to be inefficient (e.g., Zuckerman & Evans 1974; Krumholz & Tan 2007; Evans et al. 2022) because, on galactic levels, it may take ~2 Gyr to convert all molecular gas currently present in the Milky Way into stars, at the current star formation rate (e.g., Bigiel et al. 2008; Kennicutt & Evans 2012), while a simple estimate of the "free-fall SFR", allowing all molecular gas in the Galaxy to form stars in one free-fall time, would be $\sim$ 100 times larger than the observed one. As a consequence, some works have considered star formation to be a "slow" process (e.g., Krumholz & Tan 2007; Evans et al. 2021, 2022). This argument is at the core of the turbulent picture of molecular cloud dynamical evolution, in which molecular clouds, having large Jeans numbers, have low star formation efficiencies because they are assumed to be supported against collapse by supersonic turbulent motions over several free-fall times.

Krumholz & McKee (2005) introduced the parameter $\epsilon_{ff}$ (eq. 3) as a measure of the star formation efficiency over one free-fall time, picturing clouds as entities that live many free-fall times supported against collapse by turbulence and magnetic fields and have a constant SFR. In this way, if a cloud had an efficiency per free-fall time of $\epsilon_{ff} \sim 0.01$, the present efficiency after the assumed time span of a cloud (~10 free-fall times, see e.g., Krumholz et al. 2019), would be SFE $\sim$ 0.1, compatible with observational estimations

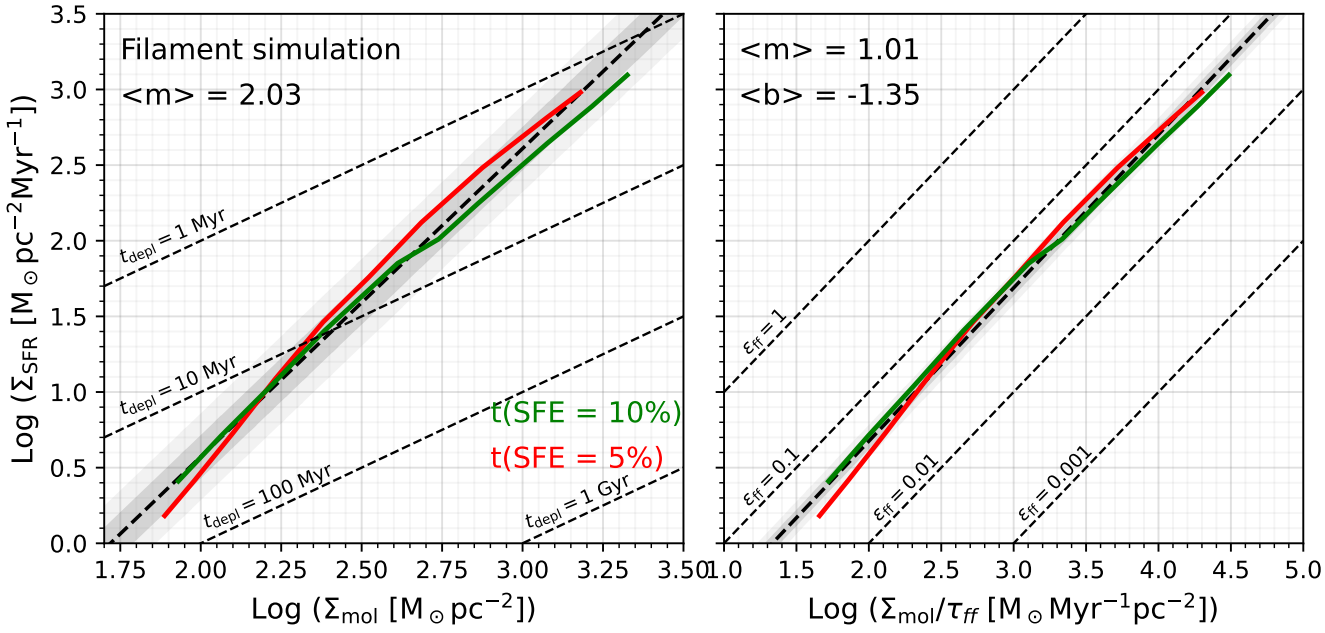


**Figure 5.** Same as Fig. 4, but for the simulated Filament.

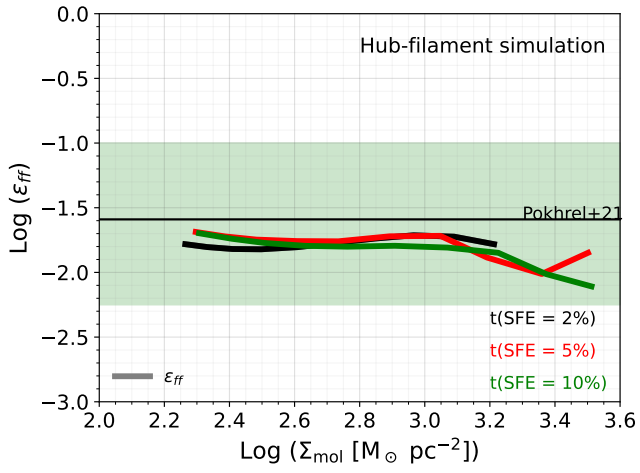


**Figure 6.** The $\epsilon_{ff}$ as a function of surface density for the Hub-filament system measured at three different times (SFE of 2%, 5%, and 10%, represented by black, red, and green continuous thick lines, respectively). The horizontal line represents the average observational determination by Pokhrel et al. (2021). The green band represents the range of values reported by these authors.

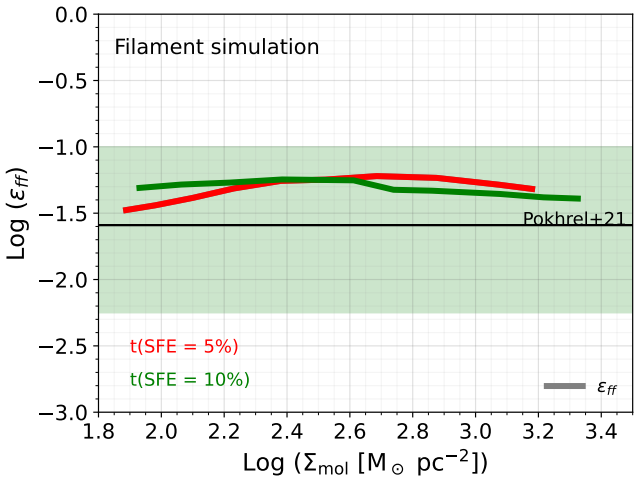


**Figure 7.** Same as Fig. 6 but for the Filament. In this case we analyze a numerical sub-box of 16 pc$^3$.

of the star formation efficiency (e.g., Myers et al. 1986). The low measured values of $\epsilon_{ff}$ have been taken as evidence that clouds not only are long-lived and supported against collapse by turbulence, but also that star formation is governed and regulated by local processes, such as turbulence or stellar feedback (e.g., Pokhrel et al. 2021; Millstone et al. 2023).

However, the GHC model (Hartmann et al. 2001; Vázquez-Semadeni et al. 2007, 2009, 2019; Heitsch & Hartmann 2008; Ballesteros-Paredes et al. 2011, 2018; Ibáñez-Mejía et al. 2017, 2022) proposes the alternative point of view that the gas within MCs is not systematically supported against collapse but rather is continuously *flowing* from the low-density regions (cold HI clouds and CO-dark molecular gas) toward the high-density ones (clumps, hub-filament systems, cores, and ultimately, stars). In this context, MCs are "segments" (stationary parts) of a continuous accretion flow from low to high density. Moreover, numerical simulations indicate that, since observationally, the clouds are defined by column density thresholds, they have an intense exchange of mass, momentum, and energy with their surrounding (Ballesteros-Paredes et al. 1999a). In particular, masses increase due to the accretion from their environment (Vázquez-Semadeni et al. 2009; González-Samaniego & Vazquez-Semadeni 2020; Camacho et al. 2020, see also the analytical model of Zamora-Avilés et al. 2012). As the clouds'

masses increase, so do their SFR and the masses of the most massive stars they contain (Zamora-Avilés & Vázquez-Semadeni 2014; Vázquez-Semadeni et al. 2017; Camacho et al. 2020; Vázquez-Semadeni et al. 2023), until massive stars capable of destroying the clouds appear several Myrs after the onset of star formation.

Within this framework, the clouds and cores appear to have long lifetimes not because they are somehow supported against collapse by some agent but rather because they continue to accrete material while they are forming stars, so that they are continuously being replenished, until the time at which they are disrupted. Indeed, there is plenty of evidence that after $\sim 5$ Myrs, a timescale that is $\sim 1.5$ times the free-fall time at densities $\sim$100 cm$^{-3}$, the characteristic density of CO molecular clouds, stars disperse their parental cloud (e.g., Herbig 1978; Leisawitz et al. 1989; Ballesteros-Paredes et al. 1999b; Hartmann et al. 2001; Ballesteros-Paredes & Hartmann 2007). This timescale is in agreement with more recent estimations of cloud lifetimes in extragalactic studies (Kruijssen et al. 2018).

#### 4.1.2 *Problems with the interpretation of $\epsilon_{\rm ff}$ as an efficiency in accreting and evolving clouds*

In the aforementioned dynamical and evolutionary context of the GHC, $\epsilon_{\rm ff}$ loses significance as an "efficiency", where by efficiency we mean the fraction of the available gas mass that is transformed into stars during one free fall time of the cloud, because of mainly two reasons:

(i) The molecular gas reservoir is not fixed but rather increases over time as the cloud accretes from its environment (e.g., Kawamura et al. 2009; Lee et al. 2016). Thus, the notion of the "available gas mass" is undefined, as the gas mass is continuously replenished.

(ii) The rate at which stars form in the clouds and clumps (the SFR) is not constant, but instead increases over time until the time when feedback from the newly-formed stars begins to erode the structures, at which point the SFR begins to decrease. Therefore, the rate at which the gas is consumed to form stars is not constant but rather varies in time.

None of these assumptions is likely to hold. In addition, it is important to notice that it is not hard to find configurations where $\epsilon_{\rm ff} > 1$ (see, e.g., Fig. 7 in Clark & Glover 2014). But by definition, an efficiency must be smaller than unity. Indeed, assuming that $\epsilon_{\rm ff}$ were an efficiency, $\epsilon_{\rm ff} > 1$ would mean that the mass converted into stars within one free-fall time would be larger than the mass available for star formation, violating mass conservation. Thus, it is best to interpret $\epsilon_{\rm ff}$ as a ratio of two *instantaneous* rates, as indicated by eq. (3).

#### 4.1.3 *The low measured values of $\epsilon_{\rm ff}$ due to the properties of a collapsing cloud*

The results from Sec. 3 show that the clouds in our simulations do exhibit low and stationary values of $\epsilon_{\rm ff}$, in agreement with observational determinations, despite the facts that *a)* the gas parcels within them are undergoing gravitational collapse flow onto the corresponding potential well and *b)* the *final* SFE is significantly larger ($\sim 10\%$) than the measured values of $\epsilon_{\rm ff}$ ($\sim 1\%$). How can this happen? A solution to this apparent conundrum can be found from the definition of $\epsilon_{\rm ff}$ in the fundamental SF law, eq. (3). In this equation, the SFR is formally given by

$$\mathrm{SFR} \equiv \frac{dM_*}{dt} \approx \frac{\Delta M_*}{\Delta t}, \tag{14}$$

so that $\epsilon_{\rm ff}$ can be written as

$$\epsilon_{\rm ff} = \left(\frac{\tau_{\rm ff}}{\Delta t}\right)\left(\frac{\Delta M_*}{M_{\rm gas}}\right). \tag{15}$$

**The problem with this approach is that, in** studies based on YSO counting, the SFR is approximated by its average value over the lifetime of the YSOs, given by the mass in YSOs divided by their typical lifetime, as indicated by eq. (5). Therefore, the *estimated* $\epsilon_{\rm ff}$ can be written as

$$\epsilon_{\rm ff} \approx \left(\frac{\tau_{\rm ff}}{\tau_{\rm YSO}}\right)\left(\frac{M_*}{M_{\rm gas}}\right). \tag{16}$$

Such an approximation is valid **in general** if the SFR is approximately constant over that time period (Dib et al. 2018). We next analyze both ratios of this equation.

of the free-fall time to the lifetime of YSOs in systems with rapidly increasing SFRs. In eq. 16, if the mass in YSOs and its time derivative, the SFR, are fast increasing, as expected for free gravitational collapse, and verified in our simulations (Figs. 3 and 8), then the time-averaging can produce a serious underestimation of the actual, current SFR. To see this, let us explicitly write the exponential growth of the mass in YSOs:

$$M_*(t) = M_0 \exp\left(\frac{t}{\tau_{\rm SFR}}\right), \tag{17}$$

where $M_0$ is some reference mass, $t$ is the time measured since the onset of star formation, and $\tau_{\rm SFR}$ is the $e$-folding time for the mass in YSOs.

This $e$-folding time can also be derived analytically by recalling the dispersion relation for the standard linear Jeans stability analysis, which reads (see, e.g., Shu 1992, eq. (8.18))

$$\omega^2 = k^2 c_{\rm s}^2 - 4\pi G \rho_0, \tag{18}$$

where $\omega \equiv 2\pi/\tau$ is the angular temporal frequency and $k = 2\pi/\lambda$ is the wavenumber of the applied perturbation, with $\tau$ being the characteristic timescale (oscillation period or $e$-folding time for stable and unstable solutions, respectively), and $\lambda$ being the wavelength of the perturbation. Instability occurs when the right-hand side of the equation is negative, and the maximum growth rate occurs at the largest scales, or vanishing $k$. In this case, the growth rate is $i\omega = i2\pi/\tau = -\sqrt{4\pi G\rho_0}$, and so the $e$-folding time, which we write as $\tau_{\rm SFR}$, is

$$\tau_{\rm SFR} = \left(\frac{\pi}{G\rho_0}\right)^{1/2}. \tag{19}$$

Comparing with the free-fall time, given by eq. (2), we see that $\tau_{\rm SFR} \approx 3.27\tau_{\rm ff}$ **(or** $\tau_{\rm ff}/\tau_{\rm SFR} \approx 0.31$**)**.

Fig. 8 shows the evolution of sinks mass (black lines) for the HFS (left) and the FS (right panel). Red lines represent the best exponential fits:

- HFS: $M_*(t) = (18.18\,M_\odot)\exp\left(\frac{t}{0.34\,\mathrm{Myr}}\right)$.
- HF: $M_*(t) = (0.23\,M_\odot)\exp\left(\frac{t}{0.61\,\mathrm{Myr}}\right)$.

Comparing with eq. 17, we can see that the $e$-folding time is $\tau_{\rm SFR} \approx 0.34$ Myr for run HFS and $\tau_{\rm SFR} \approx 0.61$ Myr for the FS (during its exponential growth phase). This implies that the free-fall time corresponding to the instantaneous SFR is $\tau_{\rm ff} \sim 0.10$ Myr for

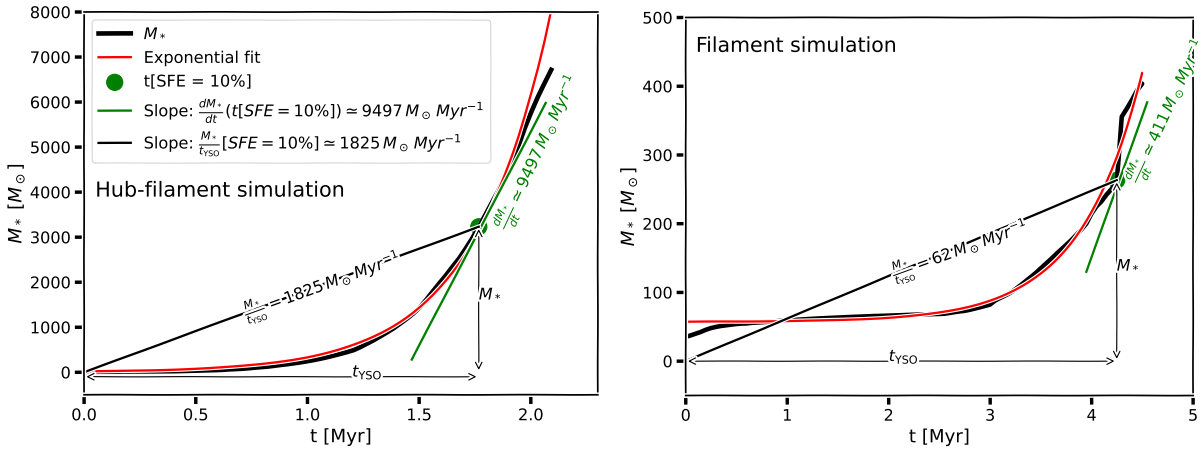


**Figure 8.** Mass of sinks as a function of time for the HFS (left panel) and the FS (right panel). The thick black lines represent direct measurements from the simulations. The red lines indicate exponential fits to the data, while the green lines show the slope at the point where the star formation efficiency (SFE) reaches 10%. Note that the average SFR (represented as $M_*/\tau_{\rm YSO}$) is necessarily lower than the instantaneous SFR ($dM_*/dt$).

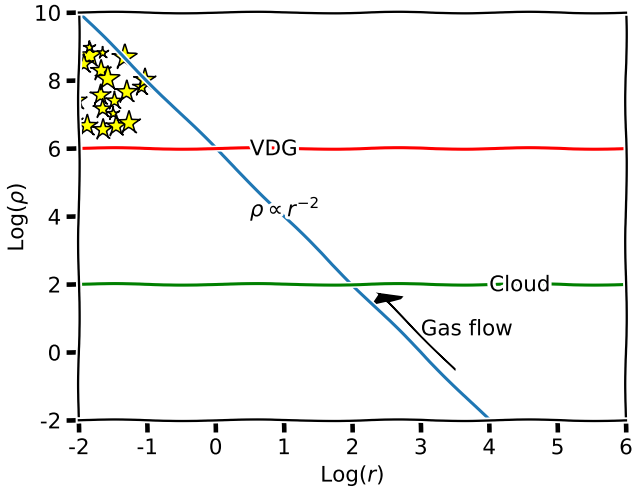


**Figure 9.** Schematic diagram illustrating a power law relationship between density and radius ($\rho \propto r^{-2}$; blue line) in arbitrary units. Horizontal lines mark specific densities: the cloud density is shown in green and the density of very dense gas (VDG) in red. Star formation within VDG is represented by yellow stars.

the HFS simulation and $\tau_{\rm ff} \sim 0.18$ Myr for the FS. Therefore, the relevant free-fall time for the present-day SFR in the HFS is $\sim 5\times$ smaller (and $\sim$2.8 $\times$ smaller for the FS) than the typically assumed lifetime of embedded YSOs ($\sim$0.5 Myr, e.g., Lada et al. 2013), and $\sim 20\times$ smaller ($\sim$11.1 $\times$ smaller for the FS) than that of general YSOs ($\sim$2 Myr, e.g., Evans et al. 2009). In our simulations, we use $\tau_{\rm YSO}$ as an observational proxy for $\tau_{\rm SFR}$, and the values of $\tau_{\rm YSO}$ used in our analysis for the HFS are $\sim$1.2, $\sim$1.5, and $\sim$1.7 Myr (see §2.1). Consequently, $\tau_{\rm ff}$ is $\sim$12, 15, and 17$\times$ larger than $\tau_{\rm ff}$, Similarly, for the FS, $\tau_{\rm YSO}$ takes the values $\sim$3.4 and 4.2 Myr, resulting in a $\tau_{\rm YSO}$ that is $\sim$18 and 23 $\times$ larger than $\tau_{\rm ff}$. Therefore, the first factor in Eq. (16) is in general small, typically of the order $\sim 0.1$. Note that this argument applies mainly to the gas directly involved in the SF process, specifically within the inner contours. In the outer contours, $\tau_{\rm ff}$ is on the order of magnitude of $\tau_{\rm YSO}$. However, while the mass in stars remains constant in the outer contours, the mass of the gas increases linearly with the contour size (see Ballesteros-Paredes 2023). This results in a net effect of maintaining a low $\epsilon_{ff}$ (see below).

**Ratio of stellar mass to gas mass.** Let us now consider the mass ratio in eq. (16). For an exponentially growing YSO population, two conditions are satisfied: First, the mass in YSOs produced over the last $e$-folding time of the currently-star-forming very dense gas (VDG) is of the order of the total mass in YSOs produced over the full SF episode.Second, the mass in just-formed YSOs is of the order of the gas mass of the VDG, since this is the gas mass that has been converted to stars in the last $e$-folding time. Therefore, we can write $M_* \sim M_{\rm VDG}$, where $M_{\rm VDG}$ is the mass of the VDG.

Now, for a near $r^{-2}$ density profile, the mass, the free-fall time, and the $e$-folding time all scale linearly with radius. Therefore, the ratio $\Delta M_*/M_{\rm gas}$ in eq. (15) is of the order of $r_{\rm VDG}/r_{\rm cloud}$, where $r_{\rm VDG}$ is the size of the currently-star-forming VDG, and $r_{\rm cloud}$ is the size of the whole region where $\epsilon_{\rm ff}$ is being evaluated. Typically, this ratio is also very small (see Fig. 9 for a schematic representation of this system).

For example, at the time when the SFE is $\sim$10%, in the HFS simulation, we identify the contour with an average density closest to $n \sim 5\times10^4$ cm$^{-3}$ and compute its mass to be $\sim$2436 $M_\odot$ (see Sec. 2.1 for details). This is $\sim 16\times$ smaller than the total mass enclosed by the outer gas surface density contour. Similarly, in the FS, the mass within the contour closest to $n \sim 4\times10^3$ cm$^{-3}$ is $\sim 506\,M_\odot$, which is $\sim 7\times$ smaller than the total mass enclosed by the outer gas surface density contour.

We can conclude then that the small *measured* value of $\epsilon_{\rm ff}$ in YSO-counting studies follows from the rapidly accelerating nature of the SFR and the fact that the gas that is actually forming stars at any given time is much denser than the mean values in the regions where $\epsilon_{\rm ff}$ is being measured. First, the very large density of the star-forming gas implies that its corresponding free-fall time is much smaller than the YSO lifetime over which the SFR is averaged. Second, the exponential growth of the SFR causes that the total mass in YSOs is given essentially by the instantaneous mass in the very-high-density region that is currently forming stars. This, together with the near-$r^{-2}$ and nearly stationary density profile of the collapsing structure, implies that the stellar mass is always much smaller than the total mass in the clouds or cores whose $\epsilon_{\rm ff}$ is being measured. Thus, the

two factors in eq. (16) are small, causing the smallness of $\epsilon_{\rm ff}$ even in regions undergoing free collapse.

#### 4.1.4 *The constancy of $\epsilon_{\rm ff}$ from gravitationally-driven accretion flow*

The *constancy* of $\epsilon_{\rm ff}$ over both time and space also remains to be explained if the clouds are undergoing free gravitational contraction. Concerning the spatial dependence, we again note, as in the previous subsection, that, for a density profile near $r^{-2}$, both $M_{\rm gas}$ and $\tau_{\rm ff}$ scale linearly with $r$, and therefore, from eq. (15), $\epsilon_{\rm ff}$ is independent of radius. This can also be seen from eq. (3), which, under the above consideration, shows that $\epsilon_{\rm ff}$ is proportional only to the instantaneous SFR. Since star formation only occurs at the density peaks, lower density isocontours around them that do not include any additional star-forming sites will have the same SFR, and thus $\epsilon_{\rm ff}$ will be independent of the isocontour's radius at any moment in time.

Moreover, the same argument applies to the temporal dependence. According to the similarity spherical collapse solution by Whitworth & Summers (1985), at large radii, where the collapse is dominated by the gravity of the gas rather than that of the stars, the density profile is given by

$$\rho t^2 \propto \left(\frac{r}{c_{\rm s} t}\right)^{-2}. \tag{20}$$

Therefore, the density profile remains independent of time for gas undergoing this type of collapse flow (see also Murray & Chang 2015). This again implies that the radial profiles of the mass and of the free-fall time are also time-independent, and therefore, so is $\epsilon_{\rm ff}$. That is, as proposed by Ballesteros-Paredes (2023), the reason for $\epsilon_{\rm ff}$, the ratio of SFR to gas-infall rate, to remain constant spatially and in time is the very collapse of the cloud. If some parts of the gas under consideration were not collapsing, $\epsilon_{\rm ff}$ would not be constant. This result can be thought of as a consequence of the fact that the rate at which the mass is transferred from one scale to the other under gravitational collapse is independent of radius for an object with an $r^{-2}$ density profile (Li 2018; Gómez et al. 2021), and it remains so during the process of collapse, as would be expected for an intrinsically phenomenon such as gravity.

We can conclude then that the spatial and temporal constancy of $\epsilon_{\rm ff}$ is due to the fact that the two factors on the right-hand-side of eq. (15) vary inversely proportional to each other with radius for a collapse-generated density profile near $r^{-2}$, and this profile is approximately stationary over time.

### 4.2 The spatially intermittent nature of star formation and the density of clusters

Another important implication of the spatially concentrated (*spatially intermittent*, in nonlinear dynamic terms) of the star formation process discussed in Sec. 4.1.3, is that star clusters appear to be significantly denser than gas clumps out of which they form (e.g., Sec. 3.4.2 and Fig. 14 of Krumholz et al. 2019). This higher density has been presented by those authors as a "problem" of the GHC scenario, but actually, Bonilla-Barroso et al. (2022) using numerical simulations (e.g., Kuznetsova et al. 2015) shown that this is a natural outcome of the GHC model. They pointed out that during the process of gravitational collapse, stellar clusters tend to develop strong density concentrations. This occurs due to a combination of

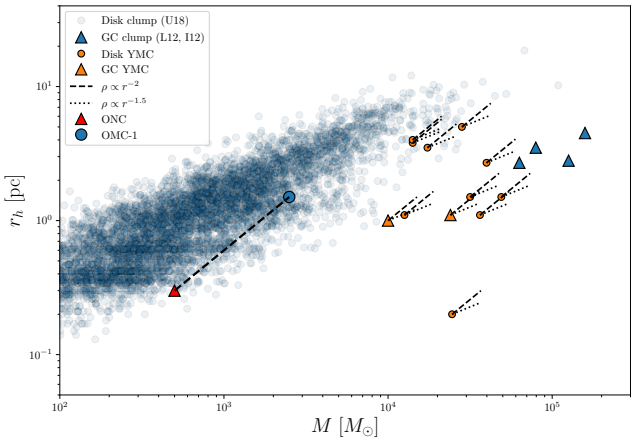


**Figure 10.** Plot of radius versus mass for gas clumps in the Galactic disk (blue light circles) from ATLASGAL, clumps near the Galactic center (blue triangles), young massive clusters (YMCs; $M > 10^4\,M_\odot$; orange circles), Galactic center YMCs (orange triangles), the Orion Nebula Cluster (ONC; red triangle) and its parent clump OMC-1 (blue circle). The black dashed and dotted lines represent the radius as a function of mass for density profiles $\rho \propto r^{-2}$ ($r \propto M$) and $\rho \propto r^{-3/2}$ ($r \propto M^{2/3}$), respectively. The black dashed line joining the ONC and OMC-1 has a slope of 1. Figure adapted from Krumholz et al. (2019, Fig. 14, see references therein).

*i)* gas starvation because stars are forming in the central collapsing region and *ii)* the incorporation of newborn stars from the surrounding vicinity. Here, we further argue that this observation may be a consequence of:

(i) the spatially intermittent nature of SF,
(ii) the continuous gas inflow to the star-forming region, and
(iii) the exponentially increasing pace of the SFR,

all of which are actually features of the GHC scenario, as dicussed above. In particular, item (i) is a consequence of item (ii); that is, the spatially intermittent nature of star formation is a direct consequence of the need for the gas to *flow* from low to high densities—i.e., from the density of the parent cloud to the density of the YSO itself. This means that the gas has to be collected from distant locations and moved into a very small region, where the density is very high. The continuous density-increasing flow manifests itself in the density profile of the collapsing gas, so that denser gas occupies smaller volume fractions. The gas forming stars at any given time (the VDG) has a density large enough that its free-fall time is much smaller than that of the parent cloud. Although the fragmentation in the region implies the appearance of multiple sites of collapse, these appear only in the VDG, not throughout the full volume of the cloud, whose lower-density parts are *flowing* towards the star forming sites.

The concentrated nature of the instantaneously-star-forming gas (the VDG) also has the implication that this mass is always a small fraction of the total cloud mass, since, as mentioned above, for a near $r^{-2}$ density profile, $M(r) \propto r$, so that the ratio of the VDG's mass ($M_{\rm VDG}$) to the cloud mass ($M_{\rm cl}$), satisfies

$$\frac{M_{\rm VDG}}{M_{\rm cl}} = \frac{r_{\rm VDG}}{r_{\rm cl}} = \frac{\tau_{\rm ff,VDG}}{\tau_{\rm ff,cl}}, \tag{21}$$

where $r_{\rm VDG}$ and $r_{\rm cl}$ are respectively the sizes of the VDG and of its parent cloud, and $\tau_{\rm ff,VDG}$ and $\tau_{\rm ff,cl}$ are their corresponding free-fall times. Since the VDG is defined as having $\tau_{\rm ff,VDG} \ll \tau_{\rm ff,cl}$, both the

mass and the size of the VDG are much smaller than those of their parent clouds, by a factor of the order of the ratio of their sizes.

Concerning item (iii) above, we have shown in Sec. 4.1.3 and Fig. 8 that the local SFR (denoted $\dot{M}_*$) in a star-forming region accelerates at a nearly exponential rate before feedback interrupts the process. As also mentioned in Sec. 4.1.3, the exponential growth of the stellar mass has two important implications: First, the current total YSO mass is comparable to the mass in YSOs formed over the last $e$-folding time of the VDG and, second, if all of the VDG's mass is converted to stars in one $e$-folding time, then the total YSO mass, $M_{\rm YSO}$, satisfies

$$M_{\rm YSO} \sim M_{\rm VDG}, \tag{22}$$

if the dense gas mass is continuously replenished by the accretion flow. Therefore, the mass density in the forming cluster is of the order of the mass density in the VDG, which, however, is much larger than the density of its parent cloud, by a factor $\sim (M_{\rm VDG}/M_{\rm cl})^{-2}$.

This is illustrated in Fig. 10 (adapted from Fig. 14 in Krumholz et al. 2019), which shows a size-mass plot for a collection of young massive clusters (orange triangles) and massive molecular clumps from the ATLASGAL survey (blue light circles Urquhart et al. 2018), as compiled by Krumholz et al. (2019), and toward lower masses we show the Orion Nebula Cluster (ONC; red rectangle) and its parent clump, OMC-1 (blue circle), in the Orion Molecular Cloud, using the data compiled by Vázquez-Semadeni et al. (2010). The black dashed lines indicate the $r \propto M$ scaling corresponding to a $\rho \propto r^{-2}$ density profile, while the black dotted lines represent $r \propto M^{2/3}$, corresponding to a density profile $\rho \propto r^{3/2}$. This figure shows that the ONC connects almost precisely with the OMC-1 clump along the $r \propto M$ line (red dashed line), being a factor $\sim 5$ smaller and less massive than the cloud and therefore a factor $\sim 25$ times denser. This suggests that the dashed lines should be extended to greater lengths and thus connect clusters with clumps that are typically $\sim 10$ times larger and more massive, and $\sim 100$ times less dense. This is also consistent with the typical final SFE observed in star-forming clouds, $\sim 10\%$, since the typical cluster mass is therefore $\sim 10\%$ of its parent clump's mass.

### 4.3 Quenching the star formation

In this paper, we have presented numerical simulations and analytical arguments concerning the establishment of the SK relation and the determination of $\epsilon_{\rm ff}$ only during the evoutionary stages dominated by infall; i.e. when feedback from locally-formed stars is negligible. Therefore, by design, our numerical simulations, which do not include feedback, are analyzed only up to moderate ($\lesssim 10\%$) *final* SFEs. Certainly, without the action of a mechanism that breaks up the cloud, our final efficiencies may grow to values substantially larger (see, e.g., Vázquez-Semadeni et al. 2010; Colín et al. 2013; Geen et al. 2017; Li et al. 2019; Grudić et al. 2019; Kim et al. 2021; Suin et al. 2023). Nevertheless, the results presented in this work without continuously driven turbulence nor stellar feedback imply that these agents are irrelevant in setting the star formation laws. Instead, the actual contribution of the stellar feedback must be shutting down the local process of collapse, by ionizing, heating up and eventually destroying the cloud, avoiding a large final efficiency of star formation. But in principle, there is no need for turbulence or feedback in settling the low values, spatial an temporal constancy of $\epsilon_{\rm ff}$. Thus, the large galactic depletion times of molecular gas are not due to star formation being "slow", but rather to it being extremely efficient in forming stars whose feedback destroys their parent cloud, preventing the present efficiency from increasing to large values.

## 5 SUMMARY AND CONCLUSIONS

In this work, we have analysed two simulated star-forming structures that evolve according to the global hierarchical collapse scenario (GHC), a Hub-filament (HFS) and a Filament (FS) that extend over up to more than 10 pc. In this scenario, MCs and their substructures can be conceptualised as *sections* of a continuous flow in which the gas is passing from low- to high-density regions, increasing in mass and density. As they grow, these structures eventually become gravitationally unstable and start to form stars at an increasing rate. The entire lifecycle of the MC, from its formation as a cold neutral cloud until its eventual destruction or dispersal by newborn massive stars, extends over a few tens of Myrs. However, once star formation initiates, these structures display relatively short lifespans, of only a few *global* free-fall times (see, e.g., Vázquez-Semadeni et al. 2019, and references therein).[7]

We have measured the Schmidt-Kennicutt (SK) type relations and the ratio of the SFR to the gas-infall rate ($\epsilon_{\rm ff}$) parameter at three early times (when the SFE is ~2, 5, and 10%), following an observationally-motivated procedure: from surface density maps, we traced closed isocontours within which we measured the average surface gas density, area, enclosed mass, mass density (and free-fall time), and the star formation rate by dividing the mass in stars by a characteristic star formation timescale defined as the period elapsed between the formation of the first sink particle and the time under analysis.

In the analysed filaments, we recovered the observed intracloud SK-type relations measured in resolved galactic clouds: the classical, $\Sigma_{\rm SFR} \propto \Sigma_{\rm mol}^2$, and the more fundamental (tighter) relation, $\Sigma_{\rm SFR} \simeq \epsilon_{\rm ff}\Sigma_{\rm mol}/\tau_{\rm ff}$ with no substantial variations among the analysed times. Even more, we also found consistency with the observations in the measured $\epsilon_{\rm ff}$. When calculating this parameter on various surface density isocontours, we obtain low values ($\epsilon_{\rm ff} \in [0.014, 0.063]$) with a distribution that is almost flat, which is consistent with recent resolved observations (e.g., Pokhrel et al. 2021).

The consistency of our results with observational determinations of the SK law and of $\epsilon_{\rm ff}$ suggests that our simulated filaments, whose evolution is mainly driven by self-gravity, capture the essential physics that determine these properties, in agreement with Ballesteros-Paredes et al. (2023), who claim that the low values of $\epsilon_{\rm ff}$ and its flat distribution in space are a consequence of collapse. In the dynamical GHC scenario, we propose the following explanations: *a)* The spatial and temporal stationarity of $\epsilon_{\rm ff}$ can be understood as a consequence of the fact that the gravitational collapse naturally develops a density slope near $\rho \propto r^{-2}$. This implies that the internal mass and the free-fall time of the structures both scale linearly with radius, (Whitworth & Summers 1985; Gómez et al. 2021), causing $\epsilon_{\rm ff}$ to be time- and radius-independent (see eq. 20 and numerical work by Quesada-Zúniga et al. 2024); *b)* The low values of $\epsilon_{\rm ff} = (M_*/M_{\rm gas})(\tau_{\rm ff}/\tau_{\rm YSO})$ (eq. 16) arise from two key factors. First, the mass of young stars ($M_*$) is limited by the gas currently forming stars at sufficiently high densities. This high-density gas is a small fraction of the total cloud mass ($M_{\rm gas}$). Second, the very dense gas that is directly involved in the process of star formation has very

[7] This free-fall time is computed using the mean density of dense gas (with $n \geqslant 100\,{\rm cm}^{-3}$) at the moment when the first sink forms within the cloud.

short free-fall time compared with the YSO lifetime, causing the ratio $\tau_{\rm ff}/\tau_{\rm YSO}$ to be small. Therefore, the two factors in the former equation that determine $\epsilon_{\rm ff}$ are small.

We also address the observation that star clusters are significantly denser than the gas clumps from which they originate, as discussed in Krumholz et al. (2019). Bonilla-Barroso et al. (2022) show that this is a natural outcome of the GHC scenario and here we further propose that three key characteristics of collapsing clouds contribute to explain this observation: *i)* the spatially intermittent nature of star formation, *ii)* the continuous replenishment of gas to the star-forming regions, and *iii)* the rapid increase in the SFR.

We also emphasise that in the GHC scenario $\epsilon_{\rm ff}$ loses significance as an efficiency over one free fall time since clouds do not have a fixed mass and the SFR is not constant, and the quantities involved in the calculation of $\epsilon_{\rm ff}$ are not measured simultaneously: the free-fall time is estimated at the present time, while the SFR (or the depletion time) is averaged over some finite timescale, such as the lifetime of the YSOs. As the SFR increases, this average underestimates the instantaneous SFR. Therefore, $\epsilon_{\rm ff}$ is only meaningful as an efficiency for static clouds with constant total mass and SFR. These conditions are not satisfied in the case of clouds undergoing GHC, with increasing masses, densities and SFRs due to gravitational contraction. Consequently, interpreting $\epsilon_{\rm ff}$ as the ratio of two instantaneous rates (the SFR to the gas-infall rate) is a more accurate approach. Interestingly, our simulations produce surprisingly low and stable values of $\epsilon_{\rm ff}$ (0.04-0.063), despite achieving significantly higher final star formation efficiencies (up to 10%).

Our results disprove the often-made suggestion that models in the GHC scenario should have large values of $\epsilon_{\rm ff}$, and offer a new perspective on the role of self-gravity in defining the star formation laws. In addition, interpretations of $\epsilon_{\rm ff}$ in observational studies should be taken with caution, as $\epsilon_{\rm ff}$ alone may not suffice to distinguish between star formation scenarios. Instead, we suggest that the distinction may be provided by evidence of accelerating star formation, and that a more meaningful efficiency is the final one after a local SF episode is terminated.

## ACKNOWLEDGEMENTS

MZA acknowledges support from CONAHCYT grant number 320772. The authors thankfully acknowledge computer resources, technical advice and support provided by: a) LANCAD and CONAHCYT on the supercomputer Miztli at DGTIC UNAM and; b) Laboratorio Nacional de Supercómputo del Sureste de México (LNS), a member of the CONAHCYT network of national laboratories. A.P. and E.V.-S. acknowledge financial support from the UNAM-PAPIIT IG100223 grant. A.P. further acknowledges support from the Sistema Nacional de Investigadores of CONAHCyT, and from the CONAHCyT project number 86372 of the 'Ciencia de Frontera 2019' program, entitled 'Citlalcóatl: A multiscale study at the new frontier of the formation and early evolution of stars and planetary systems', México.

## DATA AVAILABILITY

The data generated for this article will be shared on request to the corresponding author.

## REFERENCES

Ballesteros-Paredes J. e. a., 2023, MNRAS, submitted
Ballesteros-Paredes J., Hartmann L., 2007, Rev. Mex. Astron. Astrofis., 43, 123
Ballesteros-Paredes J., Vázquez-Semadeni E., Scalo J., 1999a, ApJ, 515, 286
Ballesteros-Paredes J., Hartmann L., Vázquez-Semadeni E., 1999b, ApJ, 527, 285
Ballesteros-Paredes J., Klessen R. S., Mac Low M. M., Vazquez-Semadeni E., 2007, in Reipurth B., Jewitt D., Keil K., eds, Protostars and Planets V. p. 63
Ballesteros-Paredes J., Hartmann L. W., Vázquez-Semadeni E., Heitsch F., Zamora-Avilés M. A., 2011, MNRAS, 411, 65
Ballesteros-Paredes J., Vázquez-Semadeni E., Palau A., Klessen R. S., 2018, MNRAS, 479, 2112
Ballesteros-Paredes et al. J., 2023, MNRAS, in prep.
Bania T. M., Lyon J. G., 1980, ApJ, 239, 173
Bigiel F., Leroy A., Walter F., Brinks E., de Blok W. J. G., Madore B., Thornley M. D., 2008, AJ, 136, 2846
Bonilla-Barroso A., et al., 2022, MNRAS, 511, 4801
Camacho V., Vázquez-Semadeni E., Palau A., Busquet G., Zamora-Avilés M., 2020, ApJ, 903, 46
Camacho V., Vázquez-Semadeni E., Palau A., Zamora-Avilés M., 2023, MNRAS, 523, 3376
Clark P. C., Glover S. C. O., 2014, MNRAS, 444, 2396
Colín P., Vázquez-Semadeni E., Gómez G. C., 2013, MNRAS, 435, 1701
Dib S., Schmeja S., Parker R. J., 2018, MNRAS, 473, 849
Dib S., et al., 2024, arXiv e-prints, p. arXiv:2405.00095
Elmegreen B. G., 2018, ApJ, 854, 16
Evans Neal J. I., et al., 2009, ApJS, 181, 321
Evans II N. J., Heiderman A., Vutisalchavakul N., 2014, ApJ, 782, 114
Evans Neal J. I., Heyer. Marc-Antoine Miville-Deschênes M., Merello Q. N.-L. M., 2021, arXiv e-prints, p. arXiv:2107.05750
Evans N. J., Kim J.-G., Ostriker E. C., 2022, ApJL, 929, L18
Federrath C., Banerjee R., Clark P. C., Klessen R. S., 2010, ApJ, 713, 269
Franco J., Cox D. P., 1986, PASP, 98, 1076
Fryxell B., et al., 2000, ApJS, 131, 273
Gallagher M. J., et al., 2018, ApJ, 858, 90
Gao Y., Solomon P. M., 2004, ApJS, 152, 63
Geen S., Soler J. D., Hennebelle P., 2017, Monthly Notices of the Royal Astronomical Society, 471, 4844
Genzel R., et al., 2010, MNRAS, 407, 2091
Gómez G. C., Vázquez-Semadeni E., Palau A., 2021, Monthly Notices of the Royal Astronomical Society, 502, 4963
González-Samaniego A., Vazquez-Semadeni E., 2020, MNRAS, 499, 668
Grudić M. Y., Hopkins P. F., Lee E. J., Murray N., Faucher-Giguère C.-A., Johnson L. C., 2019, Monthly Notices of the Royal Astronomical Society, 488, 1501
Gutermuth R. A., Pipher J. L., Megeath S. T., Myers P. C., Allen L. E., Allen T. S., 2011, ApJ, 739, 84
Hartmann L., Ballesteros-Paredes J., Bergin E. A., 2001, ApJ, 562, 852
Hartmann L., Ballesteros-Paredes J., Heitsch F., 2012, MNRAS, 420, 1457
Heiderman A., Evans Neal J. I., 2015, ApJ, 806, 231
Heiderman A., Evans II N. J., Allen L. E., Huard T., Heyer M., 2010, ApJ, 723, 1019
Heitsch F., Hartmann L., 2008, ApJ, 689, 290
Heitsch F., Burkert A., Hartmann L. W., Slyz A. D., Devriendt J. E. G., 2005, ApJL, 633, L113
Hennebelle P., Pérault M., 1999, A& A, 351, 309
Herbig G. H., 1978, in Mirzoyan L. V., ed., Problems of Physics and Evolution of the Universe.. Publishing House of the Armenian Academy of Sciences, p. 171
Heyer M., Gutermuth R., Urquhart J. S., Csengeri T., Wienen M., Leurini S., Menten K., Wyrowski F., 2016, A& A, 588, A29
Ibáñez-Mejía J. C., Mac Low M.-M., Klessen R. S., Baczynski C., 2017, ApJ, 850, 62
Ibáñez-Mejía J. C., Mac Low M.-M., Klessen R. S., 2022, ApJ, 925, 196
Juárez C., et al., 2017, ApJ, 844, 44

Kawamura A., et al., 2009, ApJS, 184, 1
Kennicutt Robert C. J., 1998, The Astrophysical Journal, 498, 541
Kennicutt R. C., Evans N. J., 2012, ARA&A, 50, 531
Kim J.-G., Ostriker E. C., Filippova N., 2021, ApJ, 911, 128
Koyama H., Inutsuka S.-i., 2002, ApJL, 564, L97
Kruijssen J. M. D., Schruba A., Hygate A. P. S., Hu C.-Y., Haydon D. T., Longmore S. N., 2018, MNRAS, 479, 1866
Krumholz M. R., McKee C. F., 2005, ApJ, 630, 250
Krumholz M. R., McKee C. F., 2020, MNRAS, 494, 624
Krumholz M. R., Tan J. C., 2007, ApJ, 654, 304
Krumholz M. R., Dekel A., McKee C. F., 2012, ApJ, 745, 69
Krumholz M. R., McKee C. F., Bland-Hawthorn J., 2019, ARA&A, 57, 227
Kuznetsova A., Hartmann L., Ballesteros-Paredes J., 2015, ApJ, 815, 27
Lada C. J., Lombardi M., Alves J. F., 2010, ApJ, 724, 687
Lada C. J., Lombardi M., Roman-Zuniga C., Forbrich J., Alves J. F., 2013, ApJ, 778, 133
Lada C. J., Lewis J. A., Lombardi M., Alves J., 2017, A& A, 606, A100
Lee E. J., Miville-Deschênes M.-A., Murray N. W., 2016, The Astrophysical Journal, 833, 229
Leisawitz D., Bash F. N., Thaddeus P., 1989, ApJS, 70, 731
Li G.-X., 2018, MNRAS, 477, 4951
Li H., Vogelsberger M., Marinacci F., Gnedin O. Y., 2019, Monthly Notices of the Royal Astronomical Society, 487, 364
Lombardi M., Bouy H., Alves J., Lada C. J., 2014, A& A, 566, A45
Mac Low M.-M., Klessen R. S., 2004, Reviews of Modern Physics, 76, 125
McKee C. F., Ostriker E. C., 2007, ARA&A, 45, 565
Millstone S., Gutermuth R., Offner S. S. R., Pokhrel R., Grudić M. Y., 2023, arXiv e-prints, p. arXiv:2310.11544
Murray N., Chang P., 2015, ApJ, 804, 44
Myers P. C., Dame T. M., Thaddeus P., Cohen R. S., Silverberg R. F., Dwek E., Hauser M. G., 1986, ApJ, 301, 398
Noriega-Mendoza H., Aguilar L. A., 2018, Rev. Mex. Astron. Astrofis., 54, 179
Ochsendorf B. B., Meixner M., Roman-Duval J., Rahman M., Evans Neal J. I., 2017, ApJ, 841, 109
Ostriker E. C., McKee C. F., Leroy A. K., 2010, ApJ, 721, 975
Padoan P., Haugbølle T., Åke Nordlund 2012, The Astrophysical Journal Letters, 759, L27
Pokhrel R., et al., 2021, ApJL, 912, L19
Quesada-Zúniga F., Zamora-Avilés M., Vázquez-Semadeni E., Gómez G. C., Ballesteros-Paredes J., 2024, to be submitted to MNRAS, X, X
Schmidt M., 1959, ApJ, 129, 243
Shu F. H., 1992, The physics of astrophysics. Volume II: Gas dynamics.
Suin P., Zavagno A., Colman T., Hennebelle P., Verliat A., Russeil D., 2023, Stellar Feedback in the Star Formation-Gas Density Relation: Comparison between Simulations and Observations (arXiv:2311.18522)
Sun J., et al., 2023, ApJL, 945, L19
Treviño-Morales S. P., et al., 2019, A& A, 629, A81
Truelove J. K., Klein R. I., McKee C. F., Holliman II J. H., Howell L. H., Greenough J. A., 1997, ApJL, 489, L179
Urquhart J. S., et al., 2018, MNRAS, 473, 1059
Vazquez-Semadeni E., Passot T., Pouquet A., 1995, ApJ, 441, 702
Vázquez-Semadeni E., Ryu D., Passot T., González R. F., Gazol A., 2006, ApJ, 643, 245
Vázquez-Semadeni E., Gómez G. C., Jappsen A. K., Ballesteros-Paredes J., González R. F., Klessen R. S., 2007, ApJ, 657, 870
Vázquez-Semadeni E., Gómez G. C., Jappsen A. K., Ballesteros-Paredes J., Klessen R. S., 2009, ApJ, 707, 1023
Vázquez-Semadeni E., Colín P., Gómez G. C., Ballesteros-Paredes J., Watson A. W., 2010, ApJ, 715, 1302
Vázquez-Semadeni E., González-Samaniego A., Colín P., 2017, MNRAS, 467, 1313
Vázquez-Semadeni E., Palau A., Ballesteros-Paredes J., Gómez G. C., Zamora-Avilés M., 2019, MNRAS, 490, 3061
Vázquez-Semadeni E., Gómez G. C., González-Samaniego A., 2023, submitted to MNRAS, X, X
Vutisalchavakul N., Evans Neal J. I., Heyer M., 2016, ApJ, 831, 73
Waagan K., Federrath C., Klingenberg C., 2011, Journal of Computational Physics, 230, 3331
Ward-Thompson D., André P., Crutcher R., Johnstone D., Onishi T., Wilson C., 2007, in Reipurth B., Jewitt D., Keil K., eds, Protostars and Planets V. p. 33 (arXiv:astro-ph/0603474), doi:10.48550/arXiv.astro-ph/0603474
Whitworth A., Summers D., 1985, MNRAS, 214, 1
Wu J., Evans Neal J. I., Gao Y., Solomon P. M., Shirley Y. L., Vanden Bout P. A., 2005, ApJL, 635, L173
Wünsch R., Walch S., Dinnbier F., Whitworth A., 2018, MNRAS, 475, 3393
Zamora-Avilés M., Vázquez-Semadeni E., 2014, ApJ, 793, 84
Zamora-Avilés M., Vázquez-Semadeni E., Colín P., 2012, ApJ, 751, 77
Zamora-Avilés M., Ballesteros-Paredes J., Hartmann L. W., 2017, MNRAS, 472, 647
Zamora-Avilés M., Vázquez-Semadeni E., Körtgen B., Banerjee R., Hartmann L., 2018, MNRAS, 474, 4824
Zari E., Lombardi M., Alves J., Lada C. J., Bouy H., 2016, A& A, 587, A106
Zuckerman B., Evans N. J. I., 1974, ApJL, 192, L149

This paper has been typeset from a TEX/LATEX file prepared by the author.